GSA DATA REPOSITORY 2013090

Supplement to

A Sagging-Spreading Continuum of Large Volcano Structure

P. K. Byrne, E. P. Holohan, M. Kervyn, B. van Wyk de Vries, V. R. Troll, J. B. Murray

MODEL SCALING

Analog models should be geometrically, kinematically, and dynamically similar to natural examples. The scaling considerations outlined here follow the approaches developed in previous experimental studies of gravitationally driven volcano spreading (Merle and Borgia, 1996; Borgia et al., 2000; Walter, 2003; Delcamp et al., 2008), but with some additions in terms of volcano sagging. We adopted a similar two-step approach: first we determined our scaling parameters in direct terms to natural systems, and then we appraised those parameters in more indirect terms via a dimensionless analysis.

Direct Scaling

For geometric scaling, we chose a model/nature length ratio of $L^* = 2 \times 10^{-6}$, such that one centimeter in the model represented five kilometers in nature. Geometric similarity was closely maintained for most parameters. The model cone radius (R_m) of 12.5 cm was scaled to a natural cone radius (R_n) of 62.5 km, a value typical of ocean island volcanoes on Earth (Watts and Zhong, 2000). The model ductile décollement thickness (P_m) of 0.5 cm scaled to a high but probably reasonable value of 2.5 km for ductile décollements in nature (see Borgia et al., 2000). A model lithosphere brittle layer thickness (B_m) of 1 to 7 cm scaled to a natural brittle thickness (B_n) of 5 to 35 km, a range identical to that observed for the seismogenic thickness of the oceanic lithosphere (see Watts and Burov, 2003). The model ductile layer thickness (D_m) of 13 cm scaled to a non-seismogenic oceanic lithosphere thickness (D_n) of 65 km, a value close to that in nature, as defined by the difference between the short-term (seismic-velocity defined) and long-term (gravity/bathymetry inferred) estimates of oceanic lithosphere thickness (see Watts and Zhong, 2000). Geometric similarity was not maintained for cone height, and hence cone shape, mainly due to limitations of space and materials available in the laboratory (discussed below). The model cone height (H_m) of 8 cm was scaled to a natural cone height (H_n) of 40 km, a value that is in excess of the true natural range (even accounting for sagging-related underestimation: see Note 1 of Table DR1). Despite this geometric difference, however, our dimensionless analysis and other arguments given below indicate that model behavior should still compare favorably to that in nature.

Dynamic similarity in analog modeling is usually expressed in terms of the model/nature stress ratio, σ*. The vertical stress in the model can be estimated from the equation

$$\sigma^* = \rho^* \times g^* \times L^*, \quad (1)$$

where ρ^*, g^*, and L^* are the model/nature ratios for density, acceleration due to gravity, and length, respectively. This calculation yields stress ratios of $\rho^* = \sim 1 \times 10^{-6}$ for Earth and $\sigma^* = \sim 3.3 \times 10^{-7}$ for Mars (Table DR1), with the difference in stress ratio for Earth and Mars arising from the latter's weaker gravitational acceleration. Both the cohesion and the internal friction coefficient of an analog material have a major influence on its integrated depth-strength profile (Schellart, 2000). The internal friction coefficient is dimensionless and is roughly equal in the model and in nature. Cohesion takes the units of stress and hence its scaling may be evaluated through σ^*. Since the cohesions of volcanic rocks range between 10^6 and 10^8 Pa, depending on alteration and fracturing (Schultz, 1996; Schellart, 2000) (Table DR1), the above stress ratios for Earth and Mars require that the brittle analog material has a cohesion of 0.3 to 100 Pa (i.e., that the analog material is 10^6 to 10^8 times mechanically weaker than a real volcano). This requirement was approximated by the use of a mixture of well-sorted fine sand (~180 μm median grain size) and 10 wt% plaster (i.e., <<100 μm) in the models, which has a cohesion, τ_0, of ~100 Pa (Donnadieu and Merle, 1998; Cecchi et al., 2005; Delcamp et al., 2008).

Kinematic similarity is considered in terms of the scaling of a variable such as viscosity, which controls the time-dependent behavior (i.e., strain rate) of the models (Donnadieu and Merle, 1998). The viscosity ratio, μ^*, may be expressed in terms of ratios for stress, σ^*, length, L^*, and velocity, S^* (Holohan et al., 2008) using the equation

$$\mu^* = (\sigma^* \times L^*) / S^*. \tag{2}$$

Taking a silicon viscosity of 5×10^4 Pa.s and an oceanic mantle viscosity in the range of 10^{20} to 10^{22} Pa.s (Watts and Zhong, 2000) yields $\mu^* = 5 \times 10^{-16}$ to 5×10^{-18}. For Earth, using these values in Equation (2) with those for $\sigma^* \times L^*$ above gives values for S^* between 4×10^3 and 4×10^5. Taking the natural subsidence rate observed at Hawaii of ca. 10^{-10} m.s^{-1} (Watts and Zhong, 2000), and solving for the expected model subsidence rate (an emergent value linked to viscosity) allowed us to determine if our models achieved kinematic similarity. The expected subsidence rate for a well-scaled model is in the range 4×10^{-7} to 4×10^{-5} m.s^{-1}, which agrees well with the observed subsidence rates of 3×10^{-6} to 3×10^{-5} m.s^{-1} (about 1 to 12 cm per hour).

Dimensionless Analysis

Geometric Sub-Division of the Experimental Data

Our scaling parameters may be considered in terms of dimensionless numbers that control whether volcano spreading or -sagging can occur and, if so, which process will predominate (Table DR2). Many of these numbers are geometric ratios that relate each part of the system to a characteristic length, in this case the cone height, H. For example, the cone shape can be described by relating cone height to cone radius, R, using the dimensionless number Π_1 (i.e., H/R).

At its most complex, the supporting basement in our models consists of an upper "décollement" portion and a lower "lithosphere" portion, each of which comprises a brittle layer overlying a ductile layer (see Fig. 2C of main article). For the upper portion of the basement, the décollement thickness, P, and décollement depth, Q, are described with the ratios Π_2 (Q/H), Π_3 (P/H), and Π_4 (Q/P). Note that this last term equates to Π_2/Π_3, and corresponds to "Π_3" of Merle and Borgia (1996). For the lower portion of the basement, the brittle lithosphere thickness, B, and ductile lithosphere thickness, D, are similarly described with the ratios Π_5 (B/H), Π_6 (D/H), and Π_7 (B/D).

For each brittle-ductile basement portion, the ratio of the cone height to ductile layer thickness, i.e., Π_3 and Π_6, determines whether the deformation style is sagging or spreading (van Wyk de Vries and Matela, 1998). The threshold ratio at which the deformation style changes is not well constrained, although earlier studies have indicated that it is viscosity-dependent (cf. Merle and Borgia, 1996; van Wyk de Vries and Matela, 1998). Nonetheless, the value of $\Pi_3 = 0.06$ we used in our experiments was sufficiently low such that the upper "décollement" portion of the basement facilitated spreading only (no sagging was observed when the lower portion remained undeformed). In contrast, the value of $\Pi_6 = 1.63$ assigned to the lower "lithosphere" portion was sufficiently high that this portion of the basement only ever facilitated sagging (no spreading-related displacements of structures were observed in experiments without an upper "décollement" portion).

Whether deformation is possible in either portion of the basement depends on the relative values of other parameters, particularly the ratio of the cone height to brittle layer thickness, i.e., Π_2 and Π_5 (Merle and Borgia, 1996). For Π_1 such as that in our models, Borgia et al. (2000) defined a theoretical parameter describing the resistance to deformation, and from this parameter defined a criterion below which deformation of a conically loaded brittle-ductile two-layer system will occur. As applied to the décollement portion of our experimental setup, this parameter is termed Π_{Spread} and the associated theoretical criterion for deformation is given by the relation

$$\Pi_{Spread} = \Pi_2 \times \Pi_4 = Q^2 / (H \times P) < 0.17. \quad (3)$$

From data of Merle and Borgia (1996), Borgia et al. (2000) ascertained the experimental value of this criterion to be $\Pi_{Spread} < 0.6 \pm 0.5$.

In our experiments featuring a décollement, Q, H, and P were set to constant values such that this criterion was always satisfied (see Table DR2), i.e., the "décollement" portion of the basement would always deform and, with a sufficiently low value for Π_2, would always spread.

For the "lithosphere" portion of the basement, $\Pi_5 \times \Pi_7 = 0.01–0.5$, a range straddling both the experimental and theoretical criteria for deformation of a brittle-ductile two-layer system. Hence, the "lithosphere" portion of the basement could remain stable or deform; if the latter, a sufficiently low value for Π_6 ensured the deformation style to be sagging. Interestingly, a notable reduction of sagging occurred in our experiments over the range $\Pi_5 \times \Pi_7 = 0.15–0.24$ (B = 4–5 cm). For those experiments with a décollement, these values coincided with the transition from sagging- to spreading-dominated deformation.

Comparison of the Experimental and Natural Systems

In terms of relating model ratios to nature, we note that our model values of $\Pi_1 = 0.64$ exceeds the upper end of the range encompassed by natural oceanic volcanoes (whose H/R values span 0.08–~0.4) (Table DR2). This is in keeping with other analog studies (cf. Merle and Borgia, 1996) and arises because it is difficult, at the laboratory scale, to evenly and consistently construct sand cones with such low slopes. For the décollement basement portion, the values of Π_2, Π_3, and Π_4 overlap with the estimated natural range. For the lithosphere portion, however, its inconsistent scaling with respect to cone height is apparent from the values of Π_5, Π_6, and Π_7, which lie at or beyond the lowermost ends of the corresponding natural ranges.

The other dimensionless numbers in Table DR2 are dynamic ratios. The brittle-ductile density ratio, Π_8, or "sink potential" (Borgia et al., 2000), of the edifice and upper lithosphere with respect to the lower lithosphere overlaps with or is a little higher than the upper end of the natural range. The remaining dynamic dimensionless ratios, Π_9, Π_{10}, and Π_{11} in the models also overlap with or closely match their corresponding estimated natural ranges. The Reynolds number, Π_{12}, in the models is several orders of magnitude higher than that estimated for nature. This is yet another limitation typical of analog studies (cf. Merle and Borgia, 1996), but the value is sufficiently low for the purposes of our experiments as the resultant flow regime in our experiments was non-turbulent (i.e., laminar).

For the "décollement" portion of the basement, the Π_{Spread} parameter can encompass the geometric spreading potential of any configuration in nature between two theoretical extremes. The first is the situation of no décollement, in which case $Q = 0$ and $P = 0$, and hence Π_{Spread} tends to infinity (i.e., infinite resistance to spreading (Borgia et al., 2000)). (A very thin décollement buried at an infinite depth relative to edifice height would also be represented by this situation.) The second theoretical extreme involves a décollement with no overburden ($B = 0$). In this scenario, $Q = 0$ but $P \neq 0$, and so Π_{Spread} tends to 0 (i.e., zero resistance to spreading). Although intermediate configurations likely abound in nature, we adopt such "on or off" conditions in our models to identify the end-member effects of Π_{Spread}. The second scenario is approximated in the models by a very thin overburden above the décollement, a condition thought to characterize oceanic island volcanoes like Hawaii and La Réunion.

To surmount the geometric scaling issues for the "lithosphere" portion we describe above, and so enable a semi-quantitative comparison to nature, we combined most of the geometric and dynamic variables that governed sagging of the volcano-basement system into one dimensionless parameter termed Π_{Sag}. This parameter relates the cone's loading of the basement to the resistance of the basement to flexure. The cone load is defined as the product of the average vertical stress at the cone base, σ_c, and the volume of the cone, V_c, where

$$\sigma_c = 0.33 \times \rho_b \times g \times H \tag{4}$$

and

$$V_c = 0.33 \times \pi \times R^2 \times H. \quad (5)$$

Note that σ_c depends only on H, whereas V_c depends on both R and H and so includes cone shape. Moreover, since it is proportional to the mass of the edifice, V_c characterizes the total force applied by the cone on the basement. The basement's resistance to loading is described in terms of the flexural rigidity of the brittle layer, F_b, which is estimated from

$$F_b = (E \times B^3) / 12\ (1\text{-}v^2), \quad (6)$$

where E is Young's modulus and v is Poisson's ratio (Watts and Zhong, 2000, and references therein). Note that F_b is proportional to B^3, and may thus be very strongly affected by even small changes in the brittle layer thickness. The dimensionless sagging parameter, Π_{Sag}, is thus defined as

$$\Pi_{Sag} = (\sigma_c \times V_c)/F_b \quad (7)$$

or

$$\Pi_{Sag} = (4.11 \times \rho \times g \times R^2 \times H^2)\ (1\text{-}v^2) / (E \times B^3). \quad (8)$$

We estimated a theoretical range of natural values for Π_{Sag} by considering two extreme cases: a very small cone upon a very thick basement (H = 2 km, R = 10 km, and B = 40 km) and a very large cone upon a very thin basement (H = 16 km, R = 150 km, and B = 2 km). The estimated ranges of Π_{Sag} in experiments overlap with those in nature (Table DR2).

Geophysical data from around edifices on Earth enabled us to estimate roughly Π_{Sag} values for individual volcanoes, such as Hawaii and Réunion. Similar estimates for Martian volcanoes are less easily made, primarily due to the difficulty in constraining H (although we note that gravity/topography admittance data (e.g., McGovern et al., 2002; McGovern et al., 2004; Belleguic et al., 2005) could be used to provide first-order estimates for this variable). The parameters we used to calculate Π_{Sag} for Hawaii and Réunion are given in Table DR3. In general, the greater Π_{Sag} value for Hawaii, in comparison to that for Réunion, is qualitatively consistent with the relative structural expressions of sagging versus spreading observed at these volcanoes. Further discussion of these values is provided in the main article.

This general agreement of Π_{Sag} for the analog models and for the natural examples, despite differences in cone geometry, probably reflects the influence of the cone volume and shape upon deformation behavior, as well as an overall dynamic similarity between the systems. Therefore, while we acknowledge that geometric dissimilarities between our models and our selected natural examples may lead to some differences in the detailed structural development of laboratory and real-world systems, we assume that the main structural relationships and trends will nonetheless be similar. The validity of this assumption is supported by 1) the results of experiments with lower cone slope values (e.g., 10° to 20°) for both volcano spreading (cf. Delcamp et al., 2008) and volcano sagging (Byrne, 2010), 2) the similarity between the analog model results shown here and the predictions of numerical models that imposed a very low-slope edifice geometry (e.g., McGovern and Solomon, 1993; Borgia, 1994; Van Wyk de Vries and Matela, 1998), and 3) the gross structural similarities between volcanoes with low slopes in nature (e.g., Fig. 1) and our analog model results (e.g., Fig. 3).

Table DR1. Scaling parameters used in this study.

Symbol	Parameter	Dimension	Models	Nature		Model/Nature Ratio	
		(unit)		*Earth*	*Mars*	*Earth*	*Mars*
			Volcano and Décollement				
H	Cone height[Note 1]	L (m)	8×10^{-2}	1×10^{3}–1.6×10^{4} [a,b,h]	4×10^{3}–2.5×10^{4} [c]	8×10^{-5}–5×10^{-6}	2×10^{-5}–3×10^{-6}
R	Cone radius	L (m)	1.25×10^{-1}	5×10^{3}–1×10^{5} [a]	1×10^{4}–3×10^{5} [c]	3×10^{-5}–1×10^{-6}	1×10^{-5}–4×10^{-7}
P	Décollement thickness[Note 2]	L (m)	5×10^{-3}	1–3×10^{3} [k]	?	1.7×10^{-6}–5×10^{-2}	?
Q	Décollement depth[Note 3]	L (m)	1×10^{-3}	0–1×10^{3} [l]	?	$>1.7\times10^{-6}$	?
			Sub-volcanic Lithosphere				
B	Brittle layer thickness[Note 4]	L (m)	$(1–7)\times10^{-2}$	1×10^{3}–4×10^{4} [d]	1.5×10^{4}–1.5×10^{5} [e,f]	1×10^{-5}–2×10^{-6}	$(5–7)\times10^{-7}$
ρ_b	Brittle material density[Note 5]	M.L^{-3} (kg.m^{-3})	1.4×10^{3}	$(2.5–3.2)\times10^{3}$ [b,g,h]	$(3–3.4)\times10^{3}$ [e,f]	$(4.4–5.6)\times10^{-1}$	$(4.1–4.6)\times10^{-1}$
θ	Brittle friction coefficient[Note 6]	-	6.3×10^{-1}	6.5×10^{-1} [i]	6.5×10^{-1}	~1	~1
τ_0	Brittle cohesion[Note 6]	M.L^{-1}.T^{-2} (Pa)	$\sim1\times10^{2}$	10^{6}–10^{8} [j]	10^{6}–10^{8}	10^{-4}–10^{-6}	10^{-4}–10^{-6}
E	Young's modulus[Note 6]	M.L^{-1}.T^{-2} (Pa)	$\sim5\times10^{6}$ [m]	7.5×10^{10} [a]	7.5×10^{10}	1.33×10^{4}	1.33×10^{4}
v	Poisson's ratio[Note 6]	-	$\sim2\times10^{-1}$ [m]	3×10^{-1} [a]	3×10^{-1}	6.6×10^{-1}	6.6×10^{-1}
D	Ductile layer thickness	L (m)	1.3×10^{-1}	1×10^{3}–5×10^{4} [a,d]	$>10^{5}$ [f]	$<10^{-6}$	$<10^{-6}$
ρ_d	Ductile material density[Note 7]	M.L^{-3} (kg.m^{-3})	$(1–1.2)\times10^{3}$	3.3×10^{3} [a,f,g]	3.5×10^{3} [e,f]	$(3–3.6)\times10^{-1}$	$(2.9–3.4)\times10^{-1}$
μ	Ductile material viscosity[Note 7]	M.L^{-1}.T^{-1} (Pa.s)	$(4–8)\times10^{4}$	10^{20}–10^{22} [a]	10^{20}–10^{22} [e]	4×10^{-18}–8×10^{-16}	4×10^{-18}–8×10^{-16}
			Other				
g	Gravity	L.T^{-2} (m.s^{-2})	9.81	9.81	3.69	1	3.8×10^{-1}
S	Velocity of deformation[Note 8]	L.T^{-1} (m.s^{-1})	3×10^{-6}–3×10^{-5}	5×10^{-11}–1×10^{-10}	?	3×10^{4}–6×10^{5}	?

Table DR1 notes:

Note 1: *H* in nature is usually measured as the maximum elevation of the volcanic edifice above a surrounding datum, such as a "normal" depth of the sea floor (e.g., Watts and Zhong, 2000). This approach is likely to underestimate *H*, however, as it neglects the portion of the volcano height that lies below the "normal" sea floor depth. This sub-datum portion of the volcano height may lie exposed within the subsidence-induced flexural trough and/or may be buried beneath trough-infilling sediments. At Hawaii, for example, geophysical studies show that the lithosphere is down-warped by some 7 km below the volcano (Zucca et al., 1982). Therefore, while Hawaii stands at almost 9 km above the surrounding "normal" sea floor depth (Zucca et al., 1982), the true value of *H* is closer to 16 km.

Note 2: The viscosity of rocks deforming as part of a ductile décollement layer in nature (e.g., clay-rich sedimentary rocks) is thought to range from 10^{17} to 10^{22} Pa.s (Van Wyk de Vries and Matela, 1998). The upper end of this range coincides with the estimated viscosity of the mantle and so for simplicity, the viscosity of the décollement below the model cone was considered to be the same as that of the lower basement ductile layer, *D*.

Note 3: The décollement depth is taken as that below the base of the volcano. It is therefore equivalent to a thickness of brittle overburden above the décollement, excluding the volcano itself. The décollement depth is a key parameter in controlling whether a volcano deforms or not (Merle and Borgia, 1996). In our experiments, the décollement layer lay beneath a thin (~1 mm) overburden layer of sand-gypsum mix, above which sat the model edifice.

Note 4: *B* represents the strong, brittle upper part of the oceanic lithosphere. It includes the oceanic crust and a portion of the oceanic mantle. *B* on Earth can be measured as the maximum depth of earthquakes in the oceanic lithosphere. This seismogenic thickness of the oceanic lithosphere ranges between zero and 40 km and shows a good correlation with the oceanic lithosphere's long-term effective elastic thickness, a property estimated from modeling of gravity and topographic data around geologic loads (e.g., Watts and Burov, 2003). *B* for Mars is taken from similarly-derived estimates of the elastic thickness of the Martian lithosphere (McGovern et al., 2004; Belleguic et al., 2005), with the assumption that, as on Earth, the elastic thickness is approximately equivalent to the seismic thickness.

Note 5: For simplicity, the densities of the cone and the brittle layer were set be the same in the models. A similar assumption is commonly made in geophysical and numerical modeling studies of flexure related to volcano loading (e.g., McGovern and Solomon, 1993; McGovern et al., 2004; Belleguic et al., 2005). We recognize, however, that in reality oceanic volcano edifices appear to have bulk densities that are slightly less than the brittle oceanic lithosphere (cf. Zucca et al., 1982; Charvis et al., 1999).

Note 6: Values for the friction coefficient, the cohesion, Young's modulus, and Poisson's ratio of rocks on Mars are assumed to be similar to those on Earth. The model values for Young's modulus and Poisson's ratio are estimates for silty sand from soil mechanics literature (Bowles, 1996).

Note 7: We use “typical” mantle values for ductile lithosphere densities on Earth and Mars, estimated from seismic and/or gravity data. Estimates for the viscosity of the ductile lithosphere on Earth are taken from modeling studies of post-glaciation rebound and lithospheric flexure on Earth (Watts and Zhong, 2000, and references therein). Values on Mars are assumed to be similar to those on Earth. Our models featured a ductile layer density of 1,000 $kg.m^{-3}$ and a viscosity of 4×10^4 Pa.s, when the silicone was new and clean. During an experiment, sand grains became admixed into the silicon. This mixing increased the ductile layer’s bulk density and viscosity, especially over the course of numerous experiments in which the same silicon is reused. The ranges for ductile layer density and viscosity in the models shown here are estimated from measurements accounting for this effect (Delcamp et al., 2008).

Note 8: The velocity of deformation is regarded as the subsidence rate of the edifice. The model subsidence rate is estimated in the laboratory, and unlike the other variables in Table DR1, it is an output variable and not a predefined parameter. The natural subsidence rate quoted for Earth is that of the Big Island of Hawaii, and is based on data from historical and archaeological studies, as well as the geologic ages of successively submerged reefs (see Watts and Zhong, 2000, and references therein). Subsidence rates on Mars are unknown.

Table DR1 references for natural parameters:
(a) Watts and Zhong (2000); (b) Zucca et al. (1982); (c) Plescia (2004); (d) Watts and Burov (2003); (e) Belleguic et al. (2005); (f) McGovern et al. (2004); (g) Lambeck and Nakiboglu (1980); (h) Gallart et al. (1999); (i) Byerlee (1968); (j) Schultz (1996); (k) Borgia et al. (2000); (l) Merle and Borgia (1996); (m) Bowles (1996).

Table DR2. Dimensionless numbers used in this study.

Π Number		Definition	Description	Models	Nature	
This Study	*M&B (1996)*[1]				*Earth*	*Mars*
Π_1	Π_1	H/R	Volcano edifice (cone) aspect ratio	6.4×10^{-1}	8×10^{-2}–4×10^{-1} (a)	7×10^{-2}
Π_2	Π_2	Q/H	Décollement depth/Edifice height	1.3×10^{-2}	6.3×10^{-6}–1 (l)	?
Π_3		P/H	Décollement thickness/Edifice height	6×10^{-2}	6.3×10^{-7}–3 (l)	?
Π_4	Π_3	Q/P	Décollement depth/Décollement thickness	2×10^{-1}	0–1×10^{3} (l)	?
Π_5		B/H	Brittle lithosphere thickness/Edifice height	1.2×10^{-1}–8.8×10^{-1}	5×10^{-1}–1.2×10^{1} (a)	1–10
Π_6		D/H	Ductile lithosphere thickness/Edifice height	1.63	6×10^{-2}–5×10^{4}	?
Π_7		B/D	Brittle/Ductile lithosphere thickness	7.7×10^{-2}–5.4×10^{-1}	<1	?
Π_8	Π_4	ρ_b/ρ_d	Brittle/Ductile lithosphere density	1.16–1.4	7×10^{-1}–1.2 (e,g)	?
Π_9		θ	Brittle friction coefficient	6.3×10^{-1}	6.5×10^{-1} (i)	6.5×10^{-1}
Π_{10}	Π_5	$([B + H] \times g \times \rho_b) \times D / (V \times \mu)$	Potential energy/Viscous forces	8.92×10^{1}–1.5×10^{3}	5.4×10^{2}–1.3×10^{3}	?
Π_{11}	Π_6	$(\tau_0 \times B) / (V \times \mu)$	Lithosphere cohesion/Viscous forces	5.5×10^{-1}–3.89×10^{1}	2×10^{-1}–1.06×10^{1}	?
Π_{12}	Π_7	$(B^2 \times V \times \rho_b) / \mu \times D$	Reynolds number	5×10^{-10}–2.5×10^{-9}	9×10^{-26}–4×10^{-24}	?
Π_{Spread}		$\Pi_2 \times \Pi_4$	Spreading if $\Pi_{Spread} < \sim0.17$ (k)	2.5×10^{-3} or ∞	2×10^{-10}–∞ (k)	?
Π_{Sag}		$(4.11 \times \rho \times g \times R^2 \times H^2)(1-v^2) / (E \times B^3)$	Sagging parameter	8×10^{-3}–2.4	$\sim1\times10^{-5}$–1.1×10^{3}	?

References for natural parameters in this table are as for Table DR1. [1]Merle and Borgia (1996).

Table DR3. Parameters used to calculate Π_{Sag} for Hawaii and Réunion.

Parameter		**Hawaii**	**Reunion**
ρ_b		2.8×10^{3} (b)	2.8×10^{3}
g		9.81	9.81
H		1.6×10^{4} (b)	8×10^{3} (h)
R		8×10^{4} (b)	7×10^{4} (h)
E		1×10^{11} (a)	1×10^{11} (a)
B	min:	2.8×10^{4} (a)	2.7×10^{4} (a)
	max:	4×10^{4} (a)	3.7×10^{4} (a)
v		3.5×10^{-1}	3.5×10^{-1}
Π_{Sag}	min:	0.025	0.006
	max:	0.074	0.016

References for natural parameters in this table are as for Table DR1.

UNRESTRICTED DÉCOLLEMENT MODEL RESULTS

When compared to models that featured a décollement restricted to the cone's diameter, an unrestricted detachment induced some subtle changes (Fig. DR 01). Extension across the peripheral bulge was distributed in a wider zone across a greater number of fractures, while the basal discontinuity lay slightly beyond, rather than at, the initial cone base. In addition, deformation was localized along several discontinuities and small folds, inhibiting the development of a single large basal scarp and the related instability. Otherwise, the results for this setup matched those of restricted décollement models.

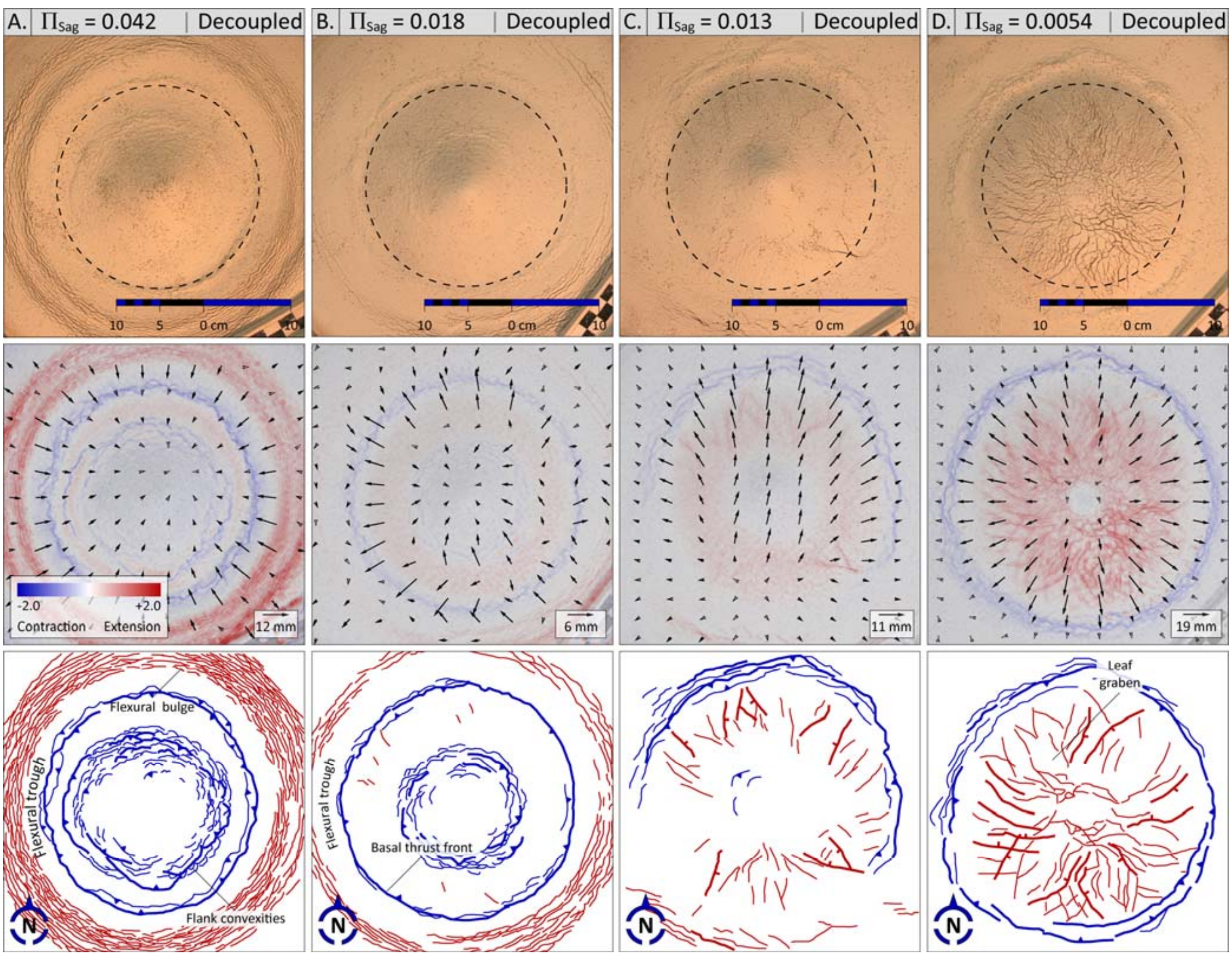

Figure DR1. Experimental results featuring a detachment that extended significantly beyond the cone's diameter. Top row: plan-view photographs of deformation (the dashed lines show the initial cone diameter); middle row: cumulative horizontal displacements and strain fields derived from PIV; bottom row: structural sketches. Red lines are normal faults (ticks on the downthrown side), while blue are reverse faults (flags on the hanging wall) (thick = major, thin = minor). Each model featured a basement-decoupled cone, and a silicone décollement thickness, *P*, of 5 mm. A. Π_{Sag} = 0.042. B. Π_{Sag} = 0.018. C. Π_{Sag} = 0.013. D. Π_{Sag} = 0.0054.

REFERENCES CITED

Belleguic, V., Lognonné, P., and Wieczorek, M., 2005 Constraints on the Martian lithosphere from gravity and topography data: Journal of Geophysical Research, v. 110, E11005.

Borgia, A., Delaney, P., and Denlinger, R., 2000, Spreading Volcanoes: Annual Review of Earth and Planetary Sciences, v. 28, p. 539–570.

Bowles, J., 1996, Foundation Analysis and Design, 5th ed.: New York, McGraw-Hill, 1,024 p.

Byerlee, J., 1968, Brittle-ductile transition in rocks: Journal of Geophysical Research, v. 73, p. 4,741–4,750.

Byrne, P. K., 2010, Volcano Flank Terraces on Mars [Ph.D. thesis]: Dublin, University of Dublin Trinity College, 256p.

Cecchi, E., van Wyk de Vries, B., and Lavest, J.-M., 2005, Flank spreading and collapse of weak-cored volcanoes: Bulletin of Volcanology, v. 67, p. 72–91.

Charvis, P., Laesanpura, A., Gallart, J., Hirn, A., Lépine, J.-C., de Voogd, B., Minshull, T., Hello, Y., and Pontoise, B., 1999, Spatial distribution of hotspot material added to the lithosphere under La Réunion, from wide-angle seismic data: Journal of Geophysical Research, v. 104, p. 2,875–2,893.

Delcamp, A., van Wyk de Vries, B., and Jones, M., 2008, The influence of edifice slope and substrata on volcano spreading: Journal of Volcanology and Geothermal Research, v.177, p. 925–943.

Donnadieu, F., and Merle, O., 1998, Experiments on the indentation process during cryptodome intrusions: New insights into Mount St. Helens deformation: Geology, v. 26, p. 79–82.

Gallart, J., Driad, L., Charvis, P., Sapin, M., Hirn, A. Diaz, J., de Voogd, B., and Sachpazi, M., 1999, Perturbation to the lithosphere along the hotspot track of La Réunion from an offshore-onshore seismic transect: Journal of Geophysical Research, v. 104, p. 2,895–2,908.

Holohan, E., Troll, V., van Wyk de Vries, B., Walsh, J., and Walter, T., 2008, Unzipping Long Valley: An explanation for vent migration patterns during an elliptical ring fracture eruption: Geology, v. 36, p. 323–326.

Lambeck, K., and Nakiboglu, S., 1980, Seamount loading and stress in the ocean lithosphere: Journal of Geophysical Research, v. 85, p. 6,403–6,418.

McGovern, P., and Solomon, S., 1993, State of stress, faulting, and eruption characteristics of large volcanoes on Mars: Journal of Geophysical Research, v. 98, p. 23,553–23,579.

McGovern, P., Solomon, S., Smith, D., Zuber, M., Simons, M., Wieczorek, M., Phillips, R., Neumann, G., Aharonson, O., and Head, J., 2002, Localized gravity/topography admittance and correlation spectra on Mars: Implications for regional and global evolution, Journal of Geophysical Research, v. 107, p. 19 1–25.

McGovern, P., Smith, J., Morgan, J., and Bulmer, M., 2004, Olympus Mons aureole deposits: new evidence for a flank failure origin: Journal of Geophysical Research, v. 107, E08008.

Merle, O., and Borgia, A., 1996, Scaled experiments of volcanic spreading: Journal of Geophysical Research, v. 101, p. 13,805–13,817.

Plescia, J., 2004, Morphometric properties of Martian volcanoes. Journal of Geophysical Research, v. 109, E03003.

Schellart, W., 2000, Shear test results for cohesion and friction coefficients for different granular materials: scaling implications for their usage in analogue modelling: Tectonophysics, v. 324, p. 1–16.

Schultz, R., 1996, Relative scale and the strength and deformability of rock masses: Journal of Structural Geology, v. 18, p. 1,139–1,149.

van Wyk de Vries, B., and Matela, R., 1998, Styles of volcano-induced deformation: numerical models of substratum flexure, spreading and extrusion: Journal of Volcanology and Geothermal Research, v. 81, p. 1–18.

Walter, T., 2003, Buttressing and fractional spreading of Tenerife, an experimental approach on the formation of rift zones: Geophysical Research Letters, v. 30, p. 29 1–4.

Watts A., and Burov, E., 2003, Lithospheric strength and its relationship to the elastic and seismogenic layer thickness: Earth and Planetary Science Letters, v. 213, p. 113–131.

Watts, A., and Zhong, S., 2000, Observations of flexure and the rheology of oceanic lithosphere: Geophysics Journal International, v. 142, p. 855–875.

Zucca, J., Hill, D., and Kovach, R., 1982, Crustal structure of Mauna Loa volcano, Hawaii, from seismic refraction and gravity data: Bulletin of the Seismological Society of America, v. 72, p. 1,535–1,550.